fluids

MDPI

Article

Numerical Analysis of the Available Power in an Overtopping Wave Energy Converter Subjected to a Sea State of the Coastal Region of Tramandaí, Brazil

Lenon A. Cisco [1], Rafael P. Maciel [2], Phelype H. Oleinik [2], Elizaldo D. dos Santos [2], Mateus N. Gomes [3], Luiz A. O. Rocha [2], Liércio A. Isoldi [2,*] and Bianca N. Machado [1]

[1] Interdisciplinary Department, Federal University of Rio Grande do Sul (UFRGS), RS 030, 11.700-km 92 Emboaba, Tramandaí 95590-000, RS, Brazil
[2] School of Engineering, Federal University of Rio Grande (FURG), Italia Av., km 8, Rio Grande 96203-900, RS, Brazil
[3] Federal Institute of Paraná (IFPR), Antônio Carlos Rodrigues Av., 453, Paranaguá 83215-750, PR, Brazil
* Correspondence: liercioisoldi@furg.br; Tel.: +55-53-99109-7356

Abstract: The present work proposes a numerical study of an overtopping wave energy converter. The goal of this study is to evaluate the theoretical power that can be converted by an overtopping device subjected to sea waves in the coastal region of Tramandaí, Brazil. For this, realistic irregular waves were generated using the WaveMIMO methodology, which allows numerical simulation of sea waves through the imposition of transient discrete data as prescribed velocity. For the numerical analysis, a two-dimensional computational model was employed using Fluent, where the device was inserted into a wave channel. The volume of the fluid multiphase model was used for the treatment of the air–water interaction. The results indicated that the free surface elevation obtained using the WaveMIMO methodology, which converts a realistic sea state into a free surface elevation series, was adequately represented. The evaluation of the theoretical power of the overtopping device during around 45 min indicated that 471.28 W was obtained. In addition, a monthly generation projection showed that this device would supply 100% of the electricity demand of a school in the city of Tramandaí. These results demonstrated that the conversion of sea wave energy into electrical energy can contribute to supplying electricity demand, especially for coastal cities.

Keywords: wave energy; computational modeling; realistic irregular waves; overtopping device; WaveMIMO methodology

check for updates

Citation: Cisco, L.A.; Maciel, R.P.; Oleinik, P.H.; dos Santos, E.D.; Gomes, M.N.; Rocha, L.A.O.; Isoldi, L.A.; Machado, B.N. Numerical Analysis of the Available Power in an Overtopping Wave Energy Converter Subjected to a Sea State of the Coastal Region of Tramandaí, Brazil. *Fluids* **2022**, *7*, 359. https://doi.org/10.3390/fluids7110359

Academic Editor: Mehrdad Massoudi

Received: 27 October 2022
Accepted: 17 November 2022
Published: 20 November 2022

Publisher's Note: MDPI stays neutral with regard to jurisdictional claims in published maps and institutional affiliations.

Copyright: © 2022 by the authors. Licensee MDPI, Basel, Switzerland. This article is an open access article distributed under the terms and conditions of the Creative Commons Attribution (CC BY) license (https://creativecommons.org/licenses/by/4.0/).

1. Introduction

The human race is on the verge of a climate crisis, announced and proved through measurements and predictions of the planet average temperature, which has increased at an accelerated rate over the last 50 years [1]. Actions to expand the energy sector with renewable sources distributed according to local potential are essential to reduce the impact of human activities on the planet. Distributed energy generation is an alternative, as it minimizes transmission losses in the electricity sector, generates local jobs, and encourages the qualification of the local workforce, which has a positive impact on the three pillars of sustainable development: environmental, social, and economic [2]. In this scenario, energy from the oceans can be harnessed as an alternative and renewable energy source.

The ocean can be compared to a reservoir with unharvested energy. Several devices have been designed and tested, with different physical operating principles and potential for harnessing the different forms of ocean energy: wave energy, tidal energy, temperature and salinity gradients, as well as energy from marine currents [3].

The irregular warming of Earth's surface, mostly covered by water, caused by the inclination of the Earth's rotation axis, is the main source of the winds. The interaction of

air masses with the ocean surface creates waves, which can vary according to the intensity of the generation event [4,5]. Beyond that, oceanic topography influences wave behavior in shallow regions [6]. A wave is a phenomenon where an energy perturbation propagates. At the sea, mechanical waves are observed, which need a physical means to propagate, in this case, the water–air interface [7].

Estimates indicate that the energy contained in ocean waves has a magnitude around 10 TW [8]. According to Falcão [9], there are three main physical principles regarding the conversion of wave energy into electrical energy: oscillating water column; oscillating bodies, which can be point absorbers or surging devices; and overtopping devices. However, this classification does not cover all the studied devices, which is the case of the submerged horizontal plate device [10–13].

Considering an overtopping wave energy converter (WEC), the goal of the present study is to use computational modeling to assess the energy potential contained in ocean waves in the coastal region of the municipality of Tramandaí, located on the northern coast of the state of Rio Grande do Sul, Brazil. To this end, firstly, realistic irregular waves and representative regular waves, concerning the sea state in this region, were numerically studied. The analysis assessed the ocean state for the date of 7 April 2019 from 12:30 p.m. to 01:30 p.m. Next, a numerical simulation of the physical operating principle of the overtopping WEC was carried out, in order to evaluate its performance when subjected to realistic irregular waves. Finally, the theoretical power obtained by the overtopping WEC was compared to real energy consumption data from a school located in the city of Tramandaí.

The present study is accomplished through computational modeling, which allows the numerical simulation of operation principles of an overtopping WEC. Numerical simulation can be defined as the process of projecting a real system into a computational model, generating analyses that can facilitate the understanding of the system behavior, allowing to evaluate operation strategies and optimize geometries [14,15].

To obtain the data used in the generation of representative regular and realistic irregular waves, the WaveMIMO methodology, presented by Machado et al. [16] and validated by Maciel et al. [17], was employed. This methodology is based on the imposition of transient discrete data as prescribed velocity, obtained in this case by means of the spectral wave model TOMAWAC (part of the Open TELEMAC-Mascaret modeling system—www.opentelemac.org, accessed on 18 August 2022). From TOMAWAC, the wave spectrum is converted into a series of free surface elevations treated and processed as wave propagation velocities in horizontal and vertical directions [16,18]. The transient discrete data, then processed as wave propagation velocity, are imposed as boundary conditions on a wave channel in Fluent. In the first stage of the study, the verification of the generation of representative regular waves was performed; in the second stage, the generation of realistic irregular waves was verified, which occurs by imposing discrete transient data of orbital velocities of wave propagation as input boundary condition; in the third and last stage, the overtopping WEC was inserted into the wave channel, where its energy potential was evaluated.

It is important to mention that numerical studies of overtopping devices considering the sea state present in the municipality of Tramandaí were not found in the literature. Despite that, numerical studies of overtopping WECs subjected to regular waves have often been developed. For example, a simulation was performed of an overtopping device against seawalls armored with artificial units [19]; a geometric evaluation was performed using Constructal Design, to investigate the effects of the relation between height and length of an overtopping device ramp and the device depth [20]; the geometry of an overtopping WEC was evaluated by means of Constructal Design when subjected to different relative depths [21]; a geometric evaluation of a three-dimensional overtopping device was performed using Constructal Design [22]; and a simulation of a multi-level overtopping device was studied [23].

As for numerical studies of overtopping WECs subjected to irregular waves, the incidence of a monochromatic wave and a wave spectrum for an overtopping device were compared [24]; the power produced by a Wave Dragon-type overtopping device subjected to irregular waves was evaluated [25]; the fluid dynamic behavior of an overtopping device subjected to regular and irregular waves was compared, finding results that indicate a larger amount of accumulated water inside the reservoir for irregular waves [26]; and the geometry of an overtopping WEC, containing either one or two ramps, was evaluated by means of Constructal Design [27]. Finally, regarding the study of the generation of irregular numerical waves, the use of OpenFoam software for fluid dynamics simulation of irregular waves was studied [28,29] and several parameters of the propagation of irregular waves in wave channels was simulated [30]. Finally, the numerical generation of long-crest irregular waves and irregular breaking waves was performed [31,32]. Despite several important works performed in the literature, little has been seen about the simulation of the realistic sea state of a particular location over an overtopping device, as done in the present work.

2. Methodology

Waves generated in fluid bodies, such as oceans, can originate from different sources. Surface waves are one of the forms of energy available in the ocean, formed mainly by the interaction between the wind and the water surface. Gravity and surface tension forces act in a restorative manner, maintaining a free surface level of the fluid and generating different shapes and types of waves, in addition to enabling their propagation [6].

To understand and model the behavior of waves, some models and theories have been developed. The modeling can be categorized as theories of regular and irregular waves, also known as deterministic and random, respectively [6]. The theory of regular waves presents waves with well-defined and constant behavior in time and space, unlike what happens with irregular waves. The main characteristics of a wave are shown in Figure 1.

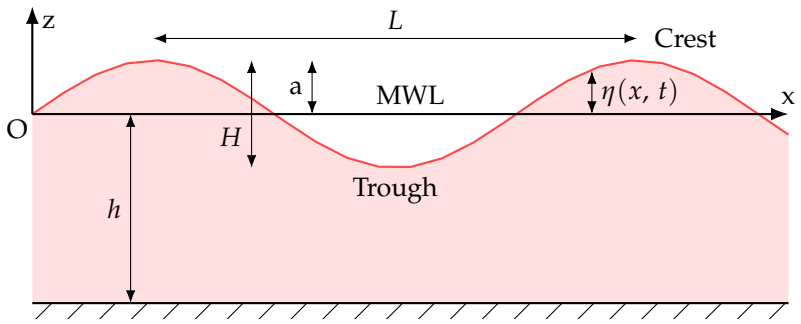

Figure 1. Wave characteristics.

In Figure 1, MWL is the mean water level, i.e., the free surface of the fluid at rest (m); crest is the highest point reached by the wave above the MWL; trough is the lowest point reached by the wave below the MWL; depth (h) is the distance between sea bottom and the MWL (m); period (T) is the time the wave takes to complete one cycle (s); amplitude (a) is the vertical distance between the crest (or trough) and the MWL (m); height (H) is the vertical distance from crest to trough (m); and, finally, wavelength (L) is the horizontal distance between two consecutive crests or troughs (m).

The elementary analytical approach to the theory of surface gravity waves is the linear wave theory or Airy theory, which can be applied to specific wave conditions that are not found in nature [33]; however, being useful for the understanding and developing of several ocean engineering investigations. In this theory, several simplifications are assumed, where the main ones are: the fluid is considered incompressible; wave generation occurs in a constant water depth; wave amplitude is very small compared to its wavelength; turbulence, viscosity, and surface tension are disregarded; and a two-dimensional and irrotational flow is assumed.

The theory solution focuses on finding the results for the free surface elevation, obtained from the following equation [6]:

$$\eta(x,\, t) = \frac{H}{2} cos(kx - \omega t) \tag{1}$$

where x is the horizontal coordinate (m) and t is time (s). In addition, the parameters wave number (k) and wave frequency (ω) are obtained from the following relationships:

$$k = \frac{2\,\pi}{L} \tag{2}$$

$$\omega = \frac{2\,\pi}{T} \tag{3}$$

The use of wave theory when modeling the problem in Fluent is given through the imposition, as boundary conditions, of the wave propagation orbital velocities in the horizontal and vertical directions. Thus, the wave propagation velocity equations, when considering the linear theory are [6]:

$$u = \frac{H}{2} \frac{gk}{\omega} \frac{cosh\ k(h+z)}{cosh(kh)} cos(kx - \omega t) \tag{4}$$

$$w = \frac{H}{2} \frac{gk}{\omega} \frac{sinh\ k(h+z)}{cosh(kh)} sin(kx - \omega t) \tag{5}$$

where u is the horizontal component of velocity (m/s), w is the vertical component of velocity (m/s), g is the gravitational acceleration (m/s^2), and z is the vertical coordinate (m). It is worth highlighting that, as mentioned, there are several wave theories; however, in this work, only the linear wave theory is presented and employed.

Other boundary conditions are imposed on the domain boundaries, which are water free surface, atmospheric pressure, and the bottom. The kinematic bottom boundary condition, considering the bottom to be stationary and impermeable, is [6]:

$$\frac{\partial \phi}{\partial z} = 0, \text{ at } z = -h \tag{6}$$

where ϕ is the velocity potential function. A kinematic boundary condition is also applied to the free surface of the fluid [6]:

$$\frac{\partial \phi}{\partial z} = \frac{\partial \eta}{\partial t}, \text{ at } z = 0 \tag{7}$$

The dynamic free surface boundary condition is [6]:

$$p_\eta = 0, \text{ at } z = 0 \tag{8}$$

where p_η represents the surface pressure. The Bernoulli equation at the surface $z = \eta$ is given by:

$$\frac{\partial \phi}{\partial t} + g\eta = 0, \text{ at } z = 0 \tag{9}$$

Lastly, the pressure outlet boundary condition was set to an atmospheric pressure value of 101,325 Pa.

2.1. Mathematical Model

The volume of fluid (VOF) method [34] is used to solve multiphase flow systems considering immiscible fluids and its main contribution was the introduction of the volumetric fraction in momentum equations. Subsequently, the method was improved and has been adopted for numerous wave energy investigations, not only for overtopping devices, but also for other types such as oscillating water column (OWC) and submerged plate [11,17,20,26,27,35].

The volumetric fraction (α) identifies the fluid present in each mesh cell, to evaluate the free surface of the flow. In this study, two phases were considered, i.e., air and water. Therefore, when $\alpha = 0$, the control volume contains only air; when $\alpha = 1$, the control volume contains only water; and when $0 < \alpha < 1$, there is a mixture of air and water in the control volume. This occurs because the sum of the volumetric fraction within a control volume is unitary [10].

The method consists of solving continuity and momentum equations for the mixture, and an additional transport equation for each phase. The VOF model equations are described below. The continuity equation for the mixture of air and water is given by [36]:

$$\frac{\partial \rho}{\partial t} + \nabla \cdot (\rho \vec{v}) = 0 \tag{10}$$

where ρ is the density of the fluid (kg/m^3) and $\vec{v}$ is the flow velocity vector (m/s). The momentum equation for the mixture is given by [36]:

$$\frac{\partial (\rho \vec{v})}{\partial t} + \nabla \cdot (\rho \vec{v} \vec{v}) = -\nabla p + \nabla \cdot (\mu \overline{\overline{\tau}}) + \rho \vec{g} + S \tag{11}$$

where p is the static pressure (Pa), $\overline{\overline{\tau}}$ is the strain rate tensor (N/m^2), μ is the dynamic viscosity (kg/ms), $\rho \vec{g}$ is the buoyancy force (N/m^3), and S is the source term representing the energy dissipation when a numerical beach is implemented. Finally, the transport equation for each of the phases is defined by [34,37]:

$$\frac{\partial \alpha_{water}}{\partial t} + \nabla \cdot (\alpha_{water} \vec{v}) = 0 \tag{12}$$

It is noteworthy that continuity and momentum equations are solved for the mixture, therefore, the viscosity and density for the mixture can be described as [34,37]:

$$\rho = \alpha \rho_{water} + (1 - \alpha) \rho_{air} \tag{13}$$

$$\mu = \alpha \mu_{water} + (1 - \alpha) \mu_{air} \tag{14}$$

The following operating conditions were considered: gravitational acceleration of 9.81 m/s^2, atmospheric pressure of 1 atm, density of air of 1.225 kg/m^3, and density of water 998.2 kg/m^3.

2.2. Numerical Model

The computational modeling used in the present study makes possible the numerical simulation of the main operating principle of an overtopping WEC, also allowing the prediction of behaviors and optimization of geometries, among other applications. Nowadays, advances in the processing and storage capacity of computers allow large-scale application of numerical techniques to solve engineering problems [15]. It is worth mentioning that the use of numerical simulation does not replace experimental research, but rather helps in predicting results and reduces the development time of systems and products.

The code that performs the steps for solving a computational fluid dynamics (CFD) problem strictly follows the conservation laws of physics. As previously mentioned, Fluent software was used in this work. Fluent is capable of performing a variety of simulations, involving flows, turbulence, heat transfer, and chemical reactions, with possibilities for academic and industrial use [38]. Based on the finite volume method (FVM), Fluent uses structured and unstructured meshes to solve the most diverse types of CFD applications.

FVM, in turn, is a way to obtain a discrete version of a partial differential equation (PDE). Its development is intrinsically linked to the concept of flow between adjacent regions or volumes, where the flow of a given quantity, such as mass or energy, is the amount of that quantity that crosses the area of a boundary. The net amount of this quantity

that crosses a control volume, per unit of time, is calculated by integrating, over these boundaries, the difference between the flows that enter and exit this volume [15].

To perform the numerical simulations using Fluent, a transient problem was considered, employing a pressure-based solver as numerical method, with the first order upwind advection scheme for the treatment of advective terms. Spatial discretization for pressure was performed using the Pressure Staggering Option method (PRESTO), a method that uses the discrete balance of continuity for an inertial control volume over the face to compute the pressure [39]. For the treatment of the volumetric fraction, the GEO-RECONSTRUCTION method was used [20,39]. The pressure–velocity coupling was solved using the Pressure-Implicit with the splitting of operators method (PISO) [40]. In addition, under-relaxation factors of 0.3 and 0.7 were imposed for continuity and momentum equations, respectively. The solutions obtained in this study were considered converged when the residuals of continuity and momentum equations in the x and z directions were lower than 10^{-3}. A verification of the numerical methods employed in this study was previously performed by Martins et al. [27], who compared results with the solution of the empirical model proposed by EurOtop [41].

2.3. Representative Regular Waves and Realistic Irregular Waves

As mentioned, the objective of this study is to evaluate, using an overtopping WEC, the energy potential that can be harnessed in the sea waves in the coastal region of the municipality of Tramandaí, located on the North Coast of the State of Rio Grande do Sul, Brazil. For this, the WaveMIMO methodology [16] was used to obtain data from the coast of Tramandaí at the point of longitude 50°6′6.86″ W and latitude 29°59′53.38″ S (see point P in Figure 2), which has a depth of 12.97 m and is located 2391.98 m from the coast.

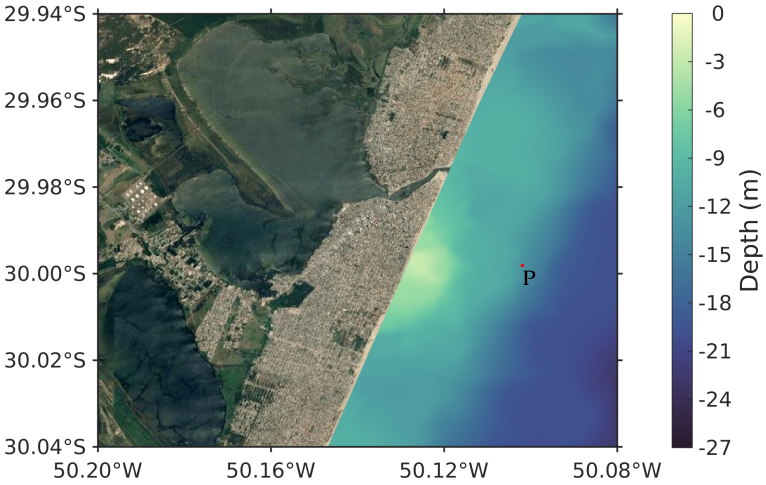

Figure 2. Satellite image with the location of the point where the data was collected.

Here, the WaveMIMO methodology was applied to a wave spectrum obtained from the spectral wave model TOMAWAC, which was transformed into a time series of free surface elevations [16,18]. TOMAWAC is an open source software capable of accurately simulating sea states of a given region. This software uses the finite element method (FEM) and considers waves generated by wind, bottom refraction, and refraction generated by currents and wave breaking dissipation, being able to calculate several parameters of interest that allow a complete description of a realistic sea state [42]. However, in TOMAWAC, it is not possible to carry out simulations of wave energy converter devices. Figure 3 presents a summary of the WaveMIMO methodology application to obtain realistic irregular waves.

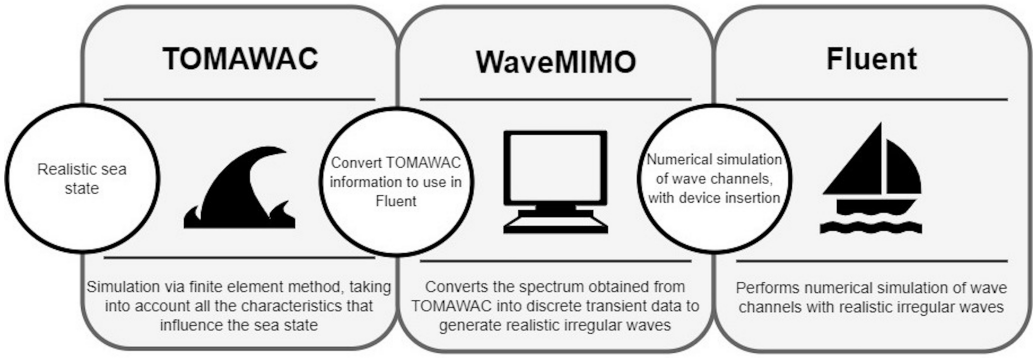

Figure 3. Process of obtaining realistic irregular waves.

The database obtained from TOMAWAC corresponds to the coast of the state of Rio Grande do Sul and part of the coast of the state of Santa Catarina, comprising the period between 1 January 2018 and 31 May 2019 [43]. Time series of significant wave height and mean wave period were extracted from the point illustrated in Figure 2 and called "Tramandaí buoy". The study was carried out in this location due to the existence of a wave motion sensor (https://www.marinha.mil.br/chm/dados-dos-ondografos/ondografos-lista, accessed on 5 September 2019) in these geographic coordinates.

For the study to have maximum representativeness and due to the fact that wave modeling requires high computational effort, it is necessary to determine a short time interval for analysis, to guarantee that it adequately represents the characteristics of the sea state in the region [44]. In this way, a statistical analysis was carried out to estimate the most frequent sea state in the study region. For this, a bivariate histogram was prepared to determine the most frequent combination of significant wave height (H_s) and mean wave period (T_m). Thus, Figure 4 shows the recurrence of sea states over the years 2018 and 2019, where it can be observed, about 2700 times, the occurrence of the sea state with $H_s \approx 0.42$ m and $T_m \approx 3.90$ s.

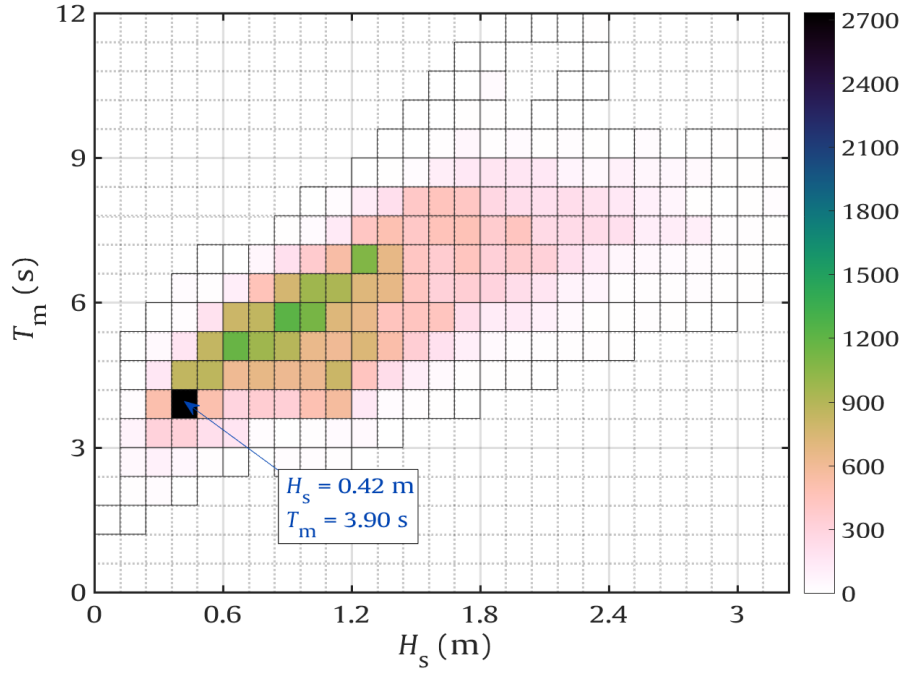

Figure 4. Histogram identifying the most frequent wave parameters during the years 2018 and 2019.

Next, the variance spectra within the pre-selected range were observed and then a spectrum with a unimodal characteristic was chosen, represented in Figure 5, occurring on

7 April 2019, at 12:30 p.m. It is worth noting that this spectrum was used to determine the characteristics of the representative regular waves, presented in Table 1.

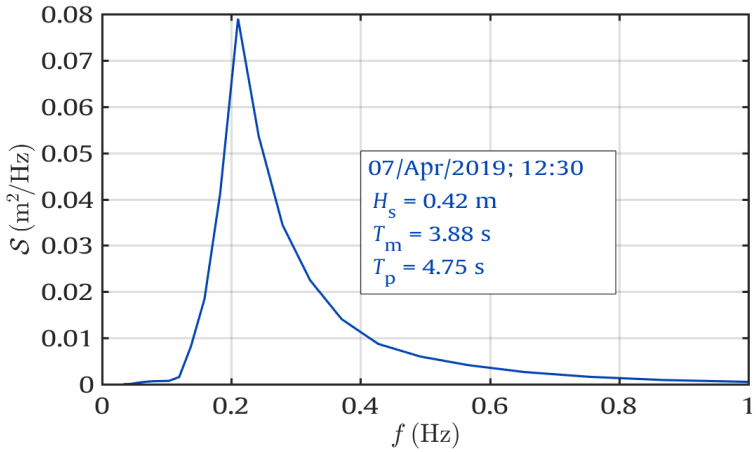

Figure 5. Representative sea state unimodal variance spectrum.

Table 1. Characteristics of the representative regular waves of Tramandaí.

Wave Parameter	Variables	Value
Period	T	3.90 s
Depth	h	12.967 m
Wave height	H	0.42 m
Wavelength	L	23.686 m

Then, the sea state spectrum is transformed into free surface elevation series, applying the inverse Fourier transform to the sea state spectrum [45]. More details about this methodology can be found in Oleinik et al. [18] and Machado et al. [16]. In Figure 6, it is possible to visualize the first 100 s of the free surface elevation time series of the representative regular waves (obtained through Equation (1)) and realistic irregular waves (obtained from TOMAWAC) of the adopted sea state (see Figures 4 and 5). As expected, representative regular waves show a stable cyclic behavior, being a simplification of the real phenomenon; while realistic irregular waves show an unstable behavior, representing more faithfully the sea state that occurs in nature. It was observed that, in general, when compared to representative regular waves, realistic irregular waves present considerable differences regarding the elevation of crests and troughs. It can also be observed that some crests and troughs of realistic irregular waves have approximately twice the amplitude of crests and troughs of representative regular waves. Finally, it is noteworthy that the waves were obtained from the unimodal variance spectrum, which occurred in the municipality of Tramandaí, Brazil, on April 7, 2019 (see Figures 4 and 5).

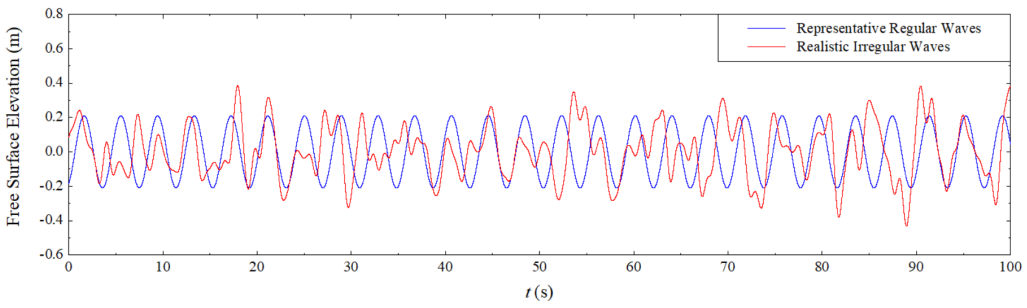

Figure 6. Realistic irregular waves and representative regular waves of the sea state which occurred in Tramandaí, Brazil.

To replicate a sea state in Fluent it was necessary to convert free surface elevation series into profiles of orbital velocities of wave propagation in vertical and horizontal directions. These orbital velocities of water particles are obtained by applying the dispersion relation equation and are imposed as boundary condition in Fluent software for the generation of realistic irregular waves [16].

2.4. Numerical Model Calibration and Case Study

Before numerically analyzing the overtopping WEC, it was necessary to identify the current wave climate in the study region so that the results have the greatest possible fidelity. To this end, this study was subdivided into three parts: in the first, the study of representative regular waves (see Table 1) was carried out, where the quality of the mesh and the time step were evaluated. It is worth mentioning that, in this case, the verification takes place through the comparison of the waves obtained numerically with the analytical expression of the linear theory (Equation (1)) for the free surface elevation; in the second part, the generation of realistic irregular waves that represent the sea state found in the coastal region of the Tramandaí was verified. In this case, the verification takes place by comparing, in the wave imposition region, free surface elevation obtained in Fluent with the elevation obtained from TOMAWAC; finally, in the third part, the operational physical principle of a sea wave energy converter device was tested. As mentioned, the device chosen was an overtopping WEC, for which the theoretical power available was determined.

2.4.1. Verification Study of the Representative Regular Waves

In this study, a two-dimensional numerical model of a real-scale wave channel was used, with dimensions following recommendations from the literature [35]. Thus, the wave channel has a length $L_C = 5L$ and a depth of $h = 12.967$ m, which is found in the coastal region of Tramandaí (see Figure 2), and an approximate total height, $H_c = 15.39$ m. Figure 7 illustrates the computational domain used to generate the representative regular waves.

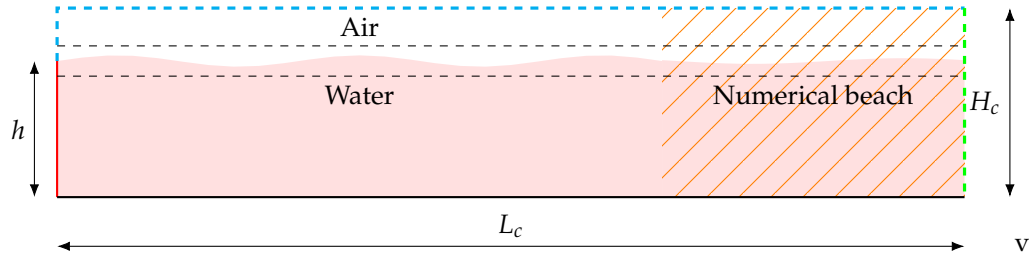

Figure 7. Illustration of the computational domain for simulation of representative regular waves.

Regarding the initial conditions, it was considered that the fluid is at rest and that the water free surface has depth h. As for the boundary conditions shown in Figure 7, on the left side of the channel (red line), a velocity inlet boundary condition was assigned, generated by the imposition of a velocity field given through Equations (4) and (5). In the upper region of the left wall of the channel, as well as on its upper surface (blue line), the pressure outlet boundary condition was assigned; on the bottom, the velocities are prescribed as zero, i.e., the non-slip and impermeability boundary conditions were adopted. Finally, on the right side (green line), the hydrostatic profile condition (pressure outlet) was imposed; this boundary condition receives a distinct nomenclature because it will act as the numerical beach (orange hatching).

The numerical beach was used by inserting a damping sink term in the momentum equation (Equation (11)) for the cell zone in the vicinity of the pressure outlet boundary, shown as the hatched region in Figure 7. This aims to reproduce damping and dissipation effects that occur on beaches when waves approach the coast and interact with the bottom [46]. Regarding wave channel simulation, a numerical beach avoids reflection of the

waves that arrive at the end of the channel, minimizing errors due to the wave channel right end wave reflection and allowing to perform longer simulations.

The source term is represented by [46]:

$$S = -\left[C_1 \rho V + \frac{1}{2} C_2 \rho |V| V\right] \left(1 - \frac{z - z_{fs}}{z_b - z_{fs}}\right) \left(\frac{x - x_s}{x_e - x_s}\right)^2 \quad (15)$$

where C_1 is the linear damping coefficient (s^{-1}), C_2 is the quadratic damping coefficient (m^{-1}), V is the fluid velocity at a given point (m/s), and z_{fs}, z_b, x_e, and x_s are the free surface, bottom, starting, and ending points of the numerical beach domain (m), respectively. It is noteworthy that recommendations from the literature were adopted [46], regarding coefficients C_1 = 20 s^{-1} and C_2 = 0, as well as the numerical beach length, which was defined as $2L$.

Regarding the spatial discretization, following recommendations from the literature [47,48], a stretched mesh was used, which applies a greater refinement in the free surface region. Thus, the computational domain was divided vertically into three regions and horizontally into one region. As for vertical discretization, the region above the free surface, which contains only air, was subdivided into 20 mesh volumes; the free surface region, which contains the air-water interface, was subdivided into 20 volumes per wave height ($H_S/20$, see Table 1); and the region below the free surface, which contains only water, was subdivided into 60 volumes. With respect to the horizontal discretization, a parameter of 50 volumes per wavelength was adopted ($L/50$, see Table 1). The discretization of the computational domain is shown in Figure 8.

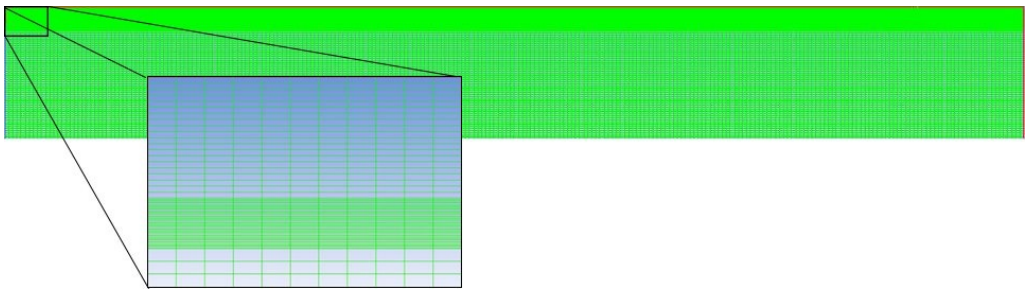

Figure 8. Illustration of domain mesh with greater refinement in the free surface region.

Since this is a transient problem, aiming to obtain greater precision with the results, tests were carried out to evaluate the quality of the time step. To evaluate time step quality, the following parameters were tested: $T/39$, $T/49$, $T/78$, $T/390$, and $T/500$, where the last parameter is indicated for studies regarding regular wave generation [35].

2.4.2. Verification Study of the Realistic Irregular Waves

The study to verify the generation of realistic irregular waves also uses a two-dimensional numerical model of a real-scale wave channel. However, in this case, the bathymetry found in the region was taken into account at the bottom of the channel (see Figure 9). Furthermore, the WaveMIMO methodology [16] presents the need to discretize the inlet region (see Figure 9, with red velocity vectors), thus enabling discrete transient data of orbital velocities of wave propagation to be imposed as boundary conditions.

It is worth noting that, in this study, the region of wave velocity imposition (red line in Figure 9) was subdivided into 20 subregions of 0.64 m each, which represents the highest free surface elevation found in the time series of realistic irregular waves. According to the recommendation for stretched meshes [47,48], it is important that the mesh in the region of free surface elevation should be refined, which corresponded to a wave height above ($+H$) and one below ($-H$) the MWL. As for the boundary conditions, it should be mentioned that they are similar to those presented in Section 2.4.1.

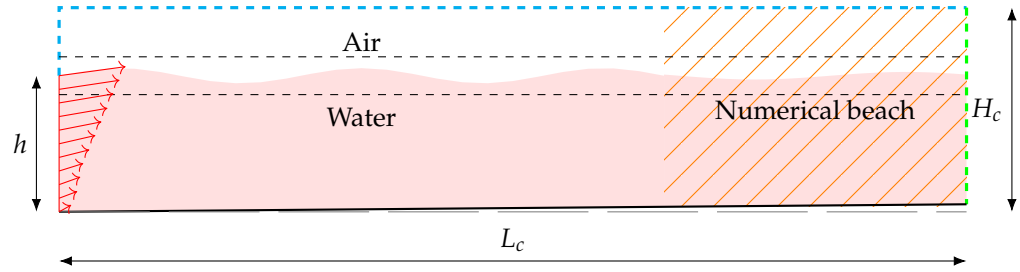

Figure 9. Illustration of the computational domain for simulation of realistic irregular waves.

Regarding the other characteristics of the wave channel (Figure 9), the dimensions adopted in the numerical model previously presented were maintained. As informed, for this study, site bathymetry was considered, which presents a difference of 0.79 m between the initial depth and the final depth of the channel. As for the spatial discretization, a stretched mesh was also used, as in the previous domain (see Figures 7 and 8). For this, the vertical discretization in the free surface region was based on the wave height of the representative regular waves, i.e., 20 mesh volumes every 0.42 m.

2.4.3. Theoretical Power Obtained by an Overtopping WEC

This study aims to evaluate the available power obtained by an overtopping WEC (see Figure 10) when subjected to a realistic sea state presented in the coastal region of Tramandaí. In this device, whose working principle is based on a reservoir raised in relation to the MWL, waves hit and climb a ramp, due to their energy, transporting volumes of water to the reservoir. The accumulated water mass, when returned to the sea, drives low head hydraulic turbines coupled to electric generators. Thus, the device converts kinetic energy from the waves into electrical energy [49].

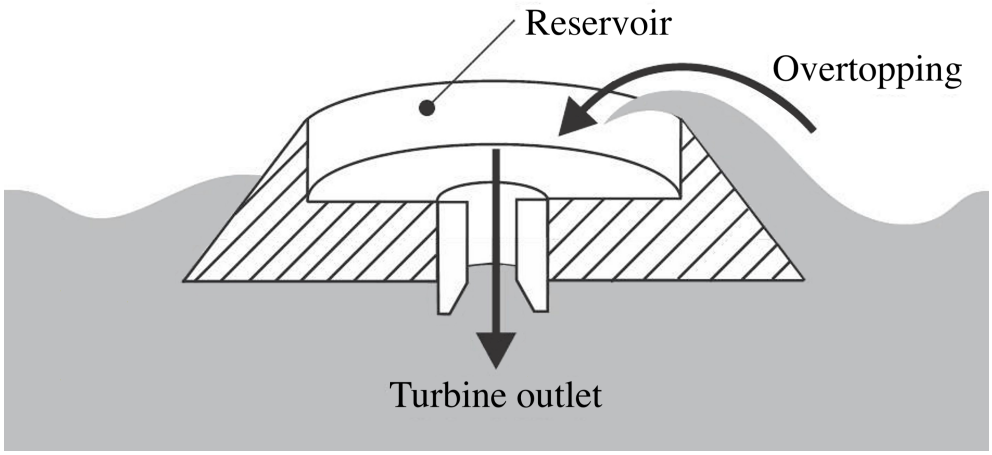

Figure 10. Physical principle of an overtopping device.

The determination of the theoretical power available in the overtopping WEC can be obtained from [20]:

$$P_a = \frac{m\, g\, h_a}{t_f} \tag{16}$$

where P_a is the available power (W), m is the mass of water in the reservoir (kg), obtained from the relationship between water density and the volume of water inside the reservoir, h_a is the water depth in the reservoir (m), and t_f is the study time interval (s). The theoretical energy, on the other hand, generated through this device can be determined from the following equation [50]:

$$E = \frac{P_a \, t_{total}}{3.6 \times 10^6} \tag{17}$$

where E is the theoretical energy generated (kWh) and t_{total} is the analyzed time period (s).

Similarly to the one described in Section 2.4.2, the computational domain consisted of a two-dimensional wave channel, with a total length $L_C = 5L$, a height $H_c = 18.39$ m (the height of the channel was increased for the insertion of the device) and water depth $h = 12.967$ m. At the beginning of the channel, the velocity inlet boundary condition region was discretized as in the irregular wave generation study, the numerical beach condition was employed at the end of the channel, and the bathymetry of the ocean was considered (see Figure 9). The device geometry was adapted from the results obtained in the previous study conducted by Martins et al. [20], where the optimal ratio between the height of the reservoir (H_1) and the base of the ramp (L_1) is $H_1/L_1 = 0.34$. Keeping this ratio as a parameter for adapting dimensions of the overtopping device, a proportionality relation was applied and the chosen parameter was the wave height. In the study performed by Martins et al. [20], wave height was $H = 1$ m. Therefore, the ratio of wave heights is 2.38.

Thus, the dimensions proposed by Martins et al. [20] for the overtopping WEC were reduced by 2.38 times, which enabled the construction of the geometry based on the optimized H_1/L_1 ratio. Hence, the dimensions of the simulated overtopping device in this study were $L_1 = 9.1147$ m, $L_R = 20$ m, and $H_1 = 3.098$ m. In addition, it is worth noting that the device is located in the channel so that, right after its reservoir, the $2L$ numerical beach begins. Regarding the boundary conditions, the same conditions as the ones employed in the generation of realistic irregular waves were imposed (see Figure 9), in addition to the non-slip and impermeability condition imposed to the walls of the overtopping device. In Figure 11, it is possible to visualize the adopted computational domain , containing the overtopping WEC.

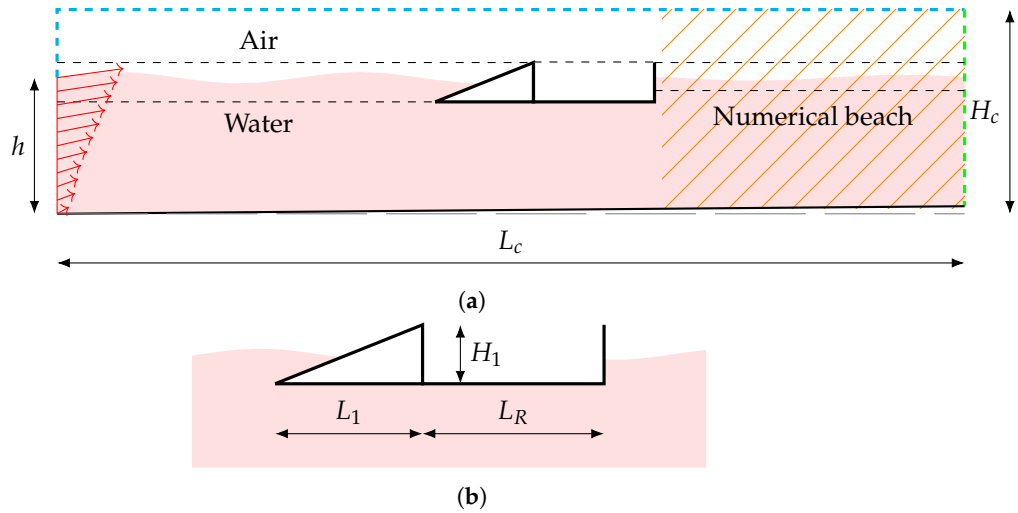

Figure 11. Illustration of the computational domain for the incidence of the realistic irregular waves over the overtopping WEC: (**a**) wave channel with device; and (**b**) device detail.

It is important to emphasize that two-dimensional studies regarding overtopping WECs have been previously performed [20,27,51–55]. This simplification is reasonable since the physical phenomenon that occurred due to the incidence of waves can be adequately approximated as an in-plane problem [26]. In addition, a two-dimensional approach can also be justified by the processing time required for the numerical simulation.

3. Results and Discussion

This section presents the results obtained for the verifications and study case analyzed in this study. It was divided into the following analyses: verification of the generation of representative regular waves, verification of the generation of realistic irregular waves, and determination of the theoretical power obtained by an overtopping WEC.

3.1. Verification Study of the Representative Regular Waves

To verify the generation of representative regular waves, the numerical solution of water free surface elevation was compared with the analytical wave obtained through Equation (1). It is worth noting that the analytically generated waves have the same characteristics as the numerical waves, which can be observed in Table 1. To compare numerical and analytical results, mean absolute error (*MAE*) and root mean square error (*RMSE*) metrics were used, according to the following equations [56]:

$$MAE = \frac{1}{n}\sum_{i=1}^{n}|y_i - \overline{y}_i| \tag{18}$$

$$RMSE = \sqrt{\frac{1}{n}\sum_{i=1}^{n}|y_i - \overline{y}_i|^2} \tag{19}$$

The results obtained for the time step analysis are shown in Table 2, where error values were calculated considering the position x = 25 m in the wave channel. Processing times for each of the cases are also presented. For all simulations, the total simulated time was t = 180 s.

Table 2. Comparison of analyzed time steps.

Time Step (s)	*MAE* (m)	*RMSE* (m)	Processing Time (h)
$T/39$	0.01447	0.01694	3.83
$T/49$	0.01351	0.01595	4.23
$T/78$	0.01255	0.01487	8.96
$T/390$	0.01091	0.01291	38.93
$T/500$	0.01075	0.01272	56.78

As can be seen in Table 2, for all analyzed time steps, *MAE* and *RMSE* values ranged from about 1.10 cm to 1.70 cm. It should be noted that time step $T/500$ presented the lowest error value, but the total processing time of this case was the longest among those studied, being 56.78 h. Meanwhile, for the $T/390$ time step, the total simulation time was reduced by approximately 31% and *MAE* and *RMSE* values did not present significant variation in relation to those obtained for the $T/500$ time step. Therefore, given the reduction of the total processing time, i.e., the reduction of the computational effort, time step $T/390$ was adopted for this study.

Figure 12 shows the comparison of the numerical wave generated in this study with the analytical wave predicted by Equation (1) at position x = 25 m. To analyze the elevation, it is worth considering two intervals in the time series. In the first, 0 s $\leq t \leq$ 15 s, it is observed that the waves start from rest and, as a function of inertia, the first crests and troughs generated in the channel are more damped, which leads to considerable deviations when compared to analytical results. Subsequently, for $t >$ 15 s, the free surface elevation of the generated numerical waves assumes a stable cyclic behavior, where *MAE* is 0.01091 m and *RMSE* is 0.01291 m. In general, it is observed that, when considering the time step $T/390$, the numerical model used in this study satisfactorily represents regular wave generation.

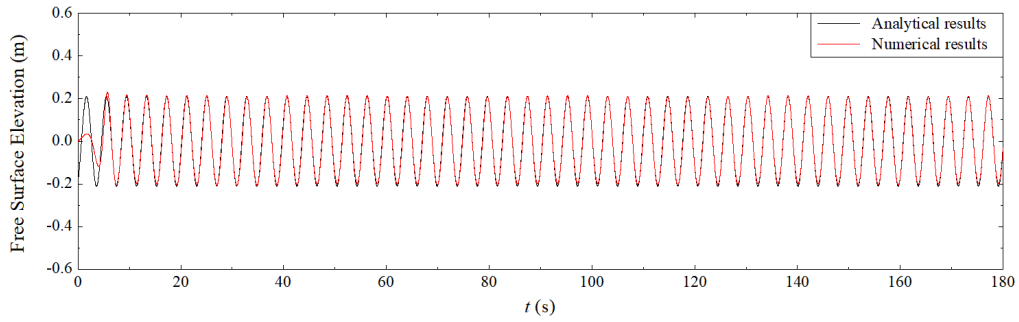

Figure 12. Verification of representative regular waves.

3.2. Verification Study of the Realistic Irregular Waves

To verify the methodology for generating realistic irregular waves, the procedure of comparing the free surface elevation obtained from TOMAWAC with the numerical solution obtained from Fluent, by using the WaveMIMO methodology, was employed. To do so, as mentioned before, the wave generation takes place through the imposition of vertical and horizontal orbital velocities of wave propagation, considering the discretization at the region of the velocity inlet boundary condition (see Figures 9 and 11). Figure 13 presents the qualitative comparison of the free surface elevation series generated through the WaveMIMO methodology in Fluent software and the series obtained from TOMAWAC. Figure 13a shows free surface elevation series over 3600 s of the simulation and Figure 13b presents the first 100 s of simulation, making it possible to visualize that the wave generated in Fluent presents an attenuation in the free surface elevation when compared to the series from TOMAWAC. It is worth noting that both series were obtained at the position $x = 0$ m of the wave channel.

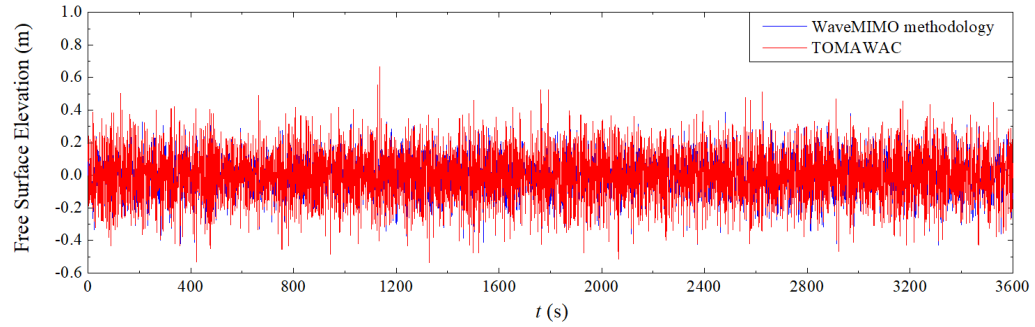

(**a**)

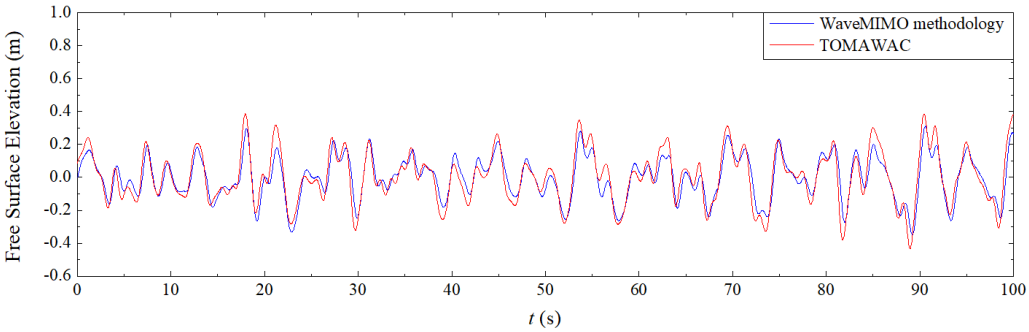

(**b**)

Figure 13. Verification of the generation of realistic irregular waves by comparing free surface elevation series obtained from the WaveMIMO methodology in Fluent and TOMAWAC considering: (**a**) 3600 s of simulation and (**b**) detail of the first 100 s of simulation.

In order to perform the quantitative analysis of the difference between both series, the values of *MAE* = 0.0534 m and *RMSE* = 0.0675 m, were calculated using Equations (18) and (19), respectively. It should be mentioned that these differences occur due to the simplifications adopted in the transformation of free surface elevation series into orbital wave velocity profiles. Furthermore, due to the initial resting condition imposed on the fluid, in Fluent. Despite these small differences, it is possible to observe in Figure 13b that the irregular waves generated in Fluent by the WaveMIMO methodology present, qualitatively, the same free surface elevation tendency obtained in TOMAWAC. In other words, the hydrodynamic model adopted adequately reproduces the irregular waves of the realistic sea state of the study region. In addition, a validation and verification of the WaveMIMO methodology can be found in Maciel et al. [17].

3.3. Determination of the Theoretical Power Obtained by an Overtopping WEC

As previously mentioned, the case study consists of numerically analyzing the water mass incident on the reservoir of an overtopping WEC, inserted in a wave channel of realistic waves, i.e., irregular waves that represent the free surface elevation existing in the coastal region of Tramandaí, Brazil, on 7 April 2019, from 12:30 p.m. to 1:14 p.m. The goal of this study is to evaluate the theoretical power obtained by this WEC device. To do so, 2673 s of simulation were considered, since, from this moment on, the reservoir of the device overflows, which can be observed in Figure 14.

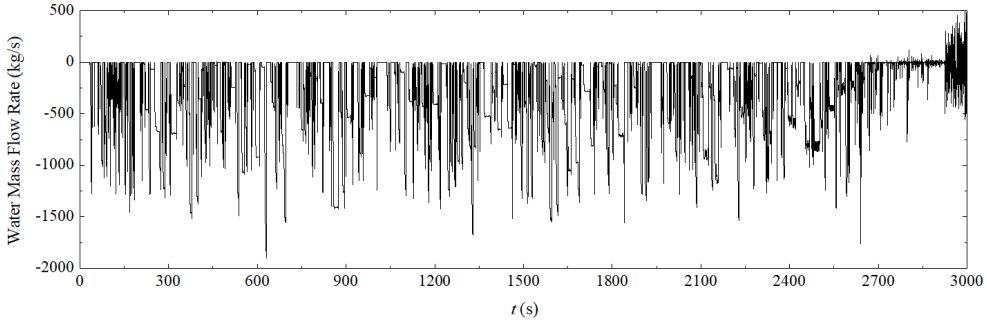

Figure 14. Instantaneous water mass flow as a function of time, considering 3000 s.

Initially, the mass flow rate (kg/s) incident in the reservoir of the overtopping device was analyzed over time. It should be noted that the monitoring of the incident water mass in the reservoir occurs through a horizontal numerical probe located at the entrance of the reservoir. As it can be seen in Figure 14, for the first seconds of simulation there was no overtopping. This was due to the generation of the first waves in the channel and the time required for them to reach and climb the device ramp. At t = 34 s, the overtopping phenomenon starts. Subsequently, for the remaining simulation time, overtopping occurs cyclically and intermittently. It should also be mentioned that the highest peak of mass flow rate occurs at approximately 630 s and the lowest at approximately 2200 s. Finally, at the end of 2673 s of simulation, an average water mass flow rate of 320.9 kg/s was observed.

Figure 15 presents the transient behavior of the time series of realistic irregular waves generated in the numerical wave channel, where it is possible to observe the water phase (in blue) and the air phase (in red). The fluid dynamic behavior was obtained for the following time instants: t = 0 s, 630 s, 2200 s, and 2673 s. For the initial instant, Figure 15a, one can visualize the initial condition of the wave channel and infer that the device reservoir does not contain water. In Figure 15b, which shows the approximate instant of occurrence of the highest overtopping discharge, it is possible to notice a mass of water accumulating inside the reservoir. In Figure 15c, the approximate time in which the lowest overtopping discharge occurs, it is possible to visualize a wave incidence on the device ramp and a greater mass of water in the reservoir. Finally, in Figure 15d, it is possible to observe the instant when the device reservoir overflows due to the volume of water.

As a means to determine the available theoretical power, given by Equation (16), the water level inside the overtopping device reservoir was measured. For this, three vertical numerical probes were used: the first, located 5 m from the reservoir left wall; the second, at the center of the reservoir; and the third, 5 m from its right wall. The mean water level monitored by the probes during the simulation can be viewed in Figure 16.

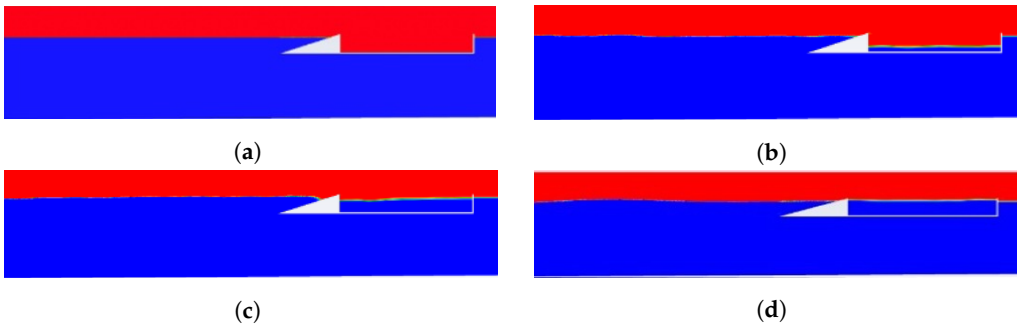

Figure 15. Transient behavior of the realistic irregular waves for the instants: (**a**) t = 0 s; (**b**) t = 630 s; (**c**) t = 2200 s; (**d**) t = 2673 s.

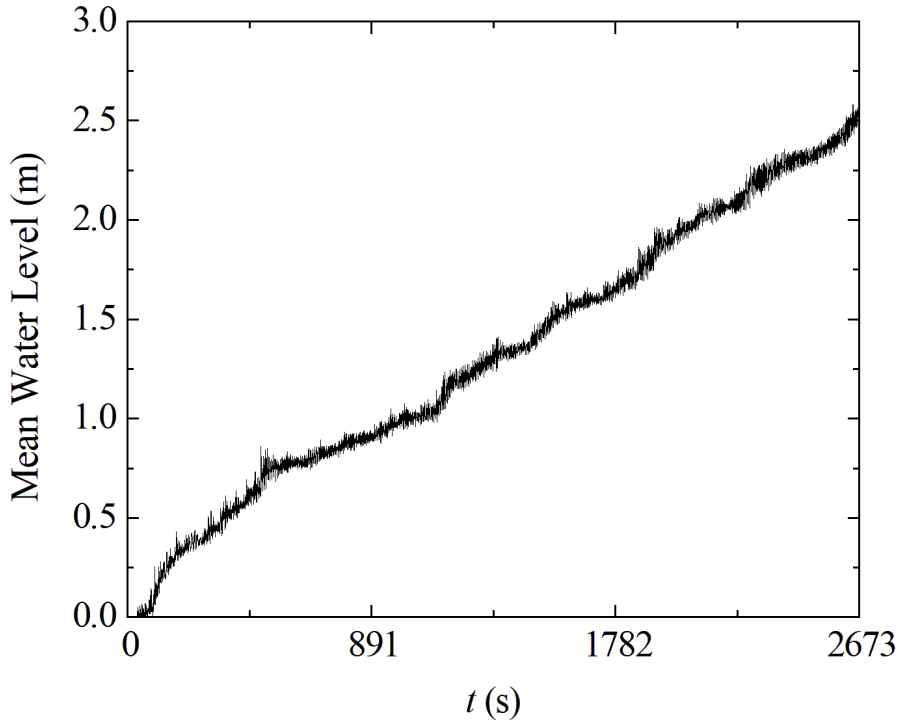

Figure 16. Mean water level inside the reservoir as a function of simulation time.

In Figure 16, there is a linear trend in the water level elevation inside the reservoir, indicating that the amount of water overtopped presents a cyclical behavior during the 2673 s of the simulation. This behavior is in agreement with those obtained in previous investigations, as in Hubner et al. [26] and Jin et al. [57]. Thus, mean water level inside the reservoir can be described by Equation (20), with an adjustment factor R^2 = 0.994:

$$H_{Int} = 0.0009\,t + 0.1344 \tag{20}$$

where H_{Int} is the mean water level inside the reservoir (m).

With H_{Int} = 2.52 m, and considering a dimension of 1 m perpendicular to the x-z plane, an accumulated mass of water of m = 50,309.28 kg was calculated along the 2673 s simulated. The time interval t_f considered for calculating the available power comprises the moment when the first overtopping occurred, t_1 = 34 s, until the moment when the

reservoir level starts to interfere with the probe, with the return of the incident water mass, t_r = 2673 s, causing data interference. Based on these values and using Equation (16), an available theoretical power of P_a = 471.28 W was found in the overtopping WEC during the analyzed time interval.

With the final goal of comparing the power obtained by the overtopping WEC to consumption data from Cândido Osório da Rosa School, located in the municipality of Tramandaí, its energy consumption data were collected between the months of December 2017 and December 2018. With these data, an average monthly consumption of 318 kWh at the school was calculated.

To make it possible to compare the theoretical power data available with the energy consumed by this educational unit, it was considered that the device acted continuously for a month under the realistic irregular waves used in this study. Under these conditions, the energy generated throughout the month, calculated by Equation (17), was E = 339.31 kWh. Therefore, the theoretical monthly generation found would be sufficient to supply 100% of the monthly energy demand of the Municipal School Cândido Osório da Rosa in the evaluated interval. It is important to highlight that this generation potential is theoretical, therefore equipment efficiency, as well as transmission and distribution energy losses were not considered.

4. Conclusions

In the present work, numerical studies were performed to evaluate the main operating principle of an overtopping WEC submitted to the sea state in the coastal region of the municipality of Tramandaí, in the state of Rio Grande do Sul, Brazil. Firstly, the computational model verification regarding the generation of regular waves representative of the sea state was performed. For this, the evaluation of time step quality was carried out. It was concluded that the evaluated time step values did not significantly influence the accuracy of the results, presenting, between the highest and the lowest time step values, *MAE* of 0.0037 m and *RMSE* of 0.0042 m; however, an augmentation of around 53 h in the processing time occurred.

In the second analysis, the computational model verification for generating realistic irregular waves was carried out. It was possible to conclude that the numerical simulation of the irregular free surface elevation series performed in Fluent, using the WaveMIMO methodology, represents adequately the time series obtained from the spectral wave model TOMAWAC. It should be noted that, qualitatively, crests and troughs presented in the simulated realistic irregular waves were adequately represented. Quantitatively, *MAE* and *RMSE* values of 0.0534 m and 0.0675 m, respectively, were found.

For the final analysis, the overtopping WEC was inserted into the wave channel and subjected to realistic irregular waves. The observation of the transient behavior demonstrated that the device behaves properly. The incident waves performed the overtopping process intermittently, allowing water accumulation in the reservoir. It was possible to conclude that the overtopping WEC analyzed in the present study obtained an available theoretical power of 471.28 W, which, based on average monthly electricity consumption and assuming a constant generation under these conditions, would supply the electricity needs of the Cândido Osório da Rosa Municipal School throughout the year 2018, which exemplifies the applicability of the present methodology for reproducing overtopping devices under real sea state conditions.

In general, the results of this work are promising and encourage further studies in the area. Among these, it can be suggested: comparing the theoretical power obtained by an overtopping WEC subjected to representative regular waves to the results of this study; comparing realistic irregular waves with sea state data obtained from a wave motion sensor; to perform a geometric optimization study of an overtopping device considering a realistic sea state; and to evaluate the theoretical power obtained by other WEC type, for instance, an OWC subjected to the incidence of realistic irregular waves.

Author Contributions: Conceptualization—L.A.C., P.H.O., L.A.I. and B.N.M.; methodology—L.A.C., P.H.O., M.N.G., L.A.O.R., E.D.d.S., B.N.M. and L.A.I.; software—M.N.G., L.A.O.R., E.D.d.S., B.N.M. and L.A.I.; validation—L.A.C., P.H.O., B.N.M. and L.A.I.; formal analysis—L.A.C., R.P.M., B.N.M. and L.A.I.; investigation—L.A.C., B.N.M. and L.A.I.; resources—B.N.M., M.N.G., L.A.O.R., E.D.d.S. and L.A.I.; data curation—L.A.C. and P.H.O.; writing (original draft preparation)—L.A.C., R.P.M., L.A.I. and B.N.M.; writing (review and editing)—R.P.M., L.A.C., L.A.I. and B.N.M.; visualization—M.N.G., L.A.O.R. and E.D.d.S.; supervision—L.A.O.R., E.D.d.S., L.A.I. and B.N.M.; project administration—L.A.O.R., E.D.d.S., L.A.I. and B.N.M.; funding acquisition—M.N.G., L.A.O.R., E.D.d.S., L.A.I. and B.N.M. All authors have read and agreed to the published version of the manuscript.

Funding: This research was funded by the Brazilian Coordination for the Improvement of Higher Education Personnel–CAPES (Finance Code 001), Research Support Foundation of the State of Rio Grande do Sul–FAPERGS (Public Call FAPERGS 07/2021 Programa Pesquisador Gaúcho–PqG, process 21/2551-0002231-0), Brazilian National Council for Scientific and Technological Development–CNPq (Processes: 309648/2021-1, 307791/2019-0, 308396/2021-9, 440010/2019-5, and 440020/2019-0) and Ministry of Science, Technology, Innovation, and Communications–MCTIC (Public Call MCTIC/CNPq Nº28/2018–Universal), and Federal University of Rio Grande do Sul–UFRGS (Public call PROPESQ/UFRGS 2019–Programa Institucional de Auxílio à Pesquisa de Docentes Recém-Contratados pela UFRGS).

Data Availability Statement: The data presented in this study are available on request from the corresponding author. The data are not publicly available due to privacy reasons.

Acknowledgments: The authors thank FAPERGS (Public Call FAPERGS 07/2021 Programa Pesquisador Gaúcho—PqG, process 21/2551-0002231-0) and CNPq (Public Call CNPQ/EQUINOR Energia Ltda Nº 38/2018, processes: 440010/2019-5 and 440020/2019-0) for the financial support. M.d.N. Gomes thanks MCTIC (Public Call MCTIC/CNPq Nº 28/2018–Universal). The authors L.A.O. Rocha, E.D. dos Santos, and L.A. Isoldi are grant holders of CNPq (processes: 307791/2019-0, 308396/2021-9, and 309648/2021-1, respectively).

Conflicts of Interest: The authors declare no conflict of interest. The funders had no role in the design of the study; in the collection, analyses, or interpretation of data; in the writing of the manuscript, or in the decision to publish the results.

References

1. IPCC. Summary for Policymakers. In *Climate Change 2013: The Physical Science Basis. Contribution of Working Group I to the Fifth Assessment Report of the Intergovernmental Panel on Climate Change*; Stocker, T., Qin, D., Plattner, G.K., Tignor, M., Allen, S., Boschung, J., Nauels, A., Xia, Y., Bex, V., Midgley, P.M., Eds.; Cambridge University Press: Cambridge, UK; New York, NY, USA, 2013; p. 1535.
2. ABGD–Associação Brasileira De Geração Distribuída. *Geração distribuída: Conceitos e Caminhos para o Desenvolvimento Sustentável*; Associação Brasileira de Geração Distribuída: São Paulo, Brazil, 2020.
3. Khan, N.; Kalair, A.; Abas, N.; Haider, A. Review of ocean tidal, wave and thermal energy technologies. *Renew. Sustain. Energy Rev.* **2017**, *72*, 590–604. [CrossRef]
4. Grimmler, J.D.A.M. Conversor de energia das ondas em energia elétrica com dispositivo de Coluna de Água Oscilante: Simulação Numérica e estudo geométrico. Master's Thesis, Universidade Federal do Rio Grande, Rio Grande, Brazil, 2013.
5. Omar, C. Estudo de métodos para a conversão da energia das ondas oceânicas. Master's Thesis, Universidade de Lisboa, Lisboa, Portugal, 2018.
6. Dean, R.G.; Dalrymple, R.A. *Water Wave Mechanics for Engineers and Scientists*; World Scientific Publishing Company: Singapore, 1991; Volume 2, p. 368.
7. de Andrade Martins, J.A. Análise de ondas em tanques de dimensões reduzidas com vistas à engenharia oceânica. Ph.D. Thesis, Escola Politécnica da Universidade de São Paulo, São Paulo, Brazil, 2003.
8. Guo, B.; Ringwood, J.V. A review of wave energy technology from a research and commercial perspective. *IET Renew. Power Gener.* **2021**, *15*, 3065–3090. [CrossRef]
9. Falcão, A.F.d.O. *The Development of Wave Energy Utilisation. IEA-OES Annual Report 2008*. Technical report; International Energy Agency Implementing Agreement on Ocean Energy Systems (IEA-OES): Lisboa, Portugal, 2008.
10. Gomes, M.d.N.; Lara, M.F.E.; Iahnke, S.L.P.; Machado, B.N.; Goulart, M.M.; Seibt, F.M.; dos Santos, E.D.; Isoldi, L.A.; Rocha, L.A.O. Numerical Approach of the Main Physical Operational Principle of Several Wave Energy Converters: Oscillating Water Column, Overtopping and Submerged Plate. *Defect Diffus. Forum* **2015**, *362*, 115–171. [CrossRef]
11. Seibt, F.; de Camargo, F.V.; Dos Santos, E.D.; Neves, M.G.; Rocha, L.A.O.; Isoldi, L.A.; Fragassa, C. Numerical evaluation on the efficiency of the submerged horizontal plate type wave energy converter. *FME Trans.* **2019**, *47*, 543–551. [CrossRef]

12. He, M.; Gao, X.; Xu, W.; Ren, B.; Wang, H. Potential application of submerged horizontal plate as a wave energy breakwater: A 2D study using the WCSPH method. *Ocean. Eng.* **2019**, *185*, 27–46. [CrossRef]
13. Wang, C.; Zhang, Y. Hydrodynamic performance of an offshore Oscillating Water Column device mounted over an immersed horizontal plate: A numerical study. *Energy* **2021**, *222*, 119964. [CrossRef]
14. Pegden, C.D.; Shannon, R.E.; Sadowski, R.P. *Introduction to Simulation Using SIMAN*, 2nd ed.; McGraw-Hill: New York, NY, USA, 1990.
15. Maliska, C.R. *Transferência de Calor e Mecânica dos Fluidos Computacional*, 2nd ed.; LTC: Rio de Janeiro, Brazil, 2004; p. 454.
16. Machado, B.N.; Oleinik, P.H.; Kirinus, E.D.P.; Santos, E.D.D.; Rocha, L.A.O.; Gomes, M.D.N.; Conde, J.M.P.; Isoldi, L.A. WaveMIMO Methodology: Numerical Wave Generation of a Realistic Sea State. *J. Appl. Comput. Mech.* **2021**, *7*, 2129–2148. [CrossRef]
17. Maciel, R.P.; Fragassa, C.; Machado, B.N.; Rocha, L.A.; Dos Santos, E.D.; Gomes, M.N.; Isoldi, L.A. Verification and validation of a methodology to numerically generate waves using transient discrete data as prescribed velocity boundary condition. *J. Mar. Sci. Eng.* **2021**, *9*, 896. [CrossRef]
18. Oleinik, P.H.; Machado, B.N.; Isoldi, L.A. Transformation of Water Wave Spectra into Time Series of Surface Elevation. *Earth* **2021**, *2*, 997–1005. [CrossRef]
19. Lu, Y.j.; Liu, H.; Wu, W.; Zhang, J.s. Numerical Simulation of Two-Dimensional Overtopping Against Seawalls Armored with Artificial Units in Regular Waves. *J. Hydrodyn.* **2007**, *19*, 322–329. [CrossRef]
20. Martins, J.C.; Goulart, M.M.; Gomes, M.d.N.; Souza, J.A.; Rocha, L.A.; Isoldi, L.A.; dos Santos, E.D. Geometric evaluation of the main operational principle of an overtopping wave energy converter by means of Constructal Design. *Renew. Energy* **2018**, *118*, 727–741. [CrossRef]
21. dos Santos, E.D.; Machado, B.N.; Zanella, M.M.; das Neves Gomes, M.; Souza, J.A.; Isoldi, L.A.; Rocha, L.A.O. Numerical Study of the Effect of the Relative Depth on the Overtopping Wave Energy Converters According to Constructal Design. *Defect Diffus. Forum* **2014**, *348*, 232–244. [CrossRef]
22. Machado, B.N. Estudo numérico tridimensional de um dispositivo de galgamento para conversão de energia das ondas do mar em energia elétrica aplicando o método Constructal Design. Ph.D. Thesis, Universidade Federal do Rio Grande do Sul, Farroupilha, Brazil, 2016.
23. Wan, Z.; Yao, Z.; Song, T.; Chen, J. Hydrodynamic characteristics of the multi-level overtopping wave power device. *J. Low Freq. Noise, Vib. Act. Control.* **2019**, *38*, 1314–1326. [CrossRef]
24. Martins, J.C.; Goulart, M.M.; Gomes, M.D.N.; Souza, J.A.; Rocha, L.A.O.; Isoldi, L.A.; Santos, E.D.D. Análise Numérica de um Dispositivo de Galgamento Onshore Comparando a Influência de uma Onda Monocromática e de um Espectro de Ondas. *Rev. Bras. Energias Renov.* **2017**, *6*. [CrossRef]
25. Rodrigues, I.A. Estudo do galgamento em conversor de ondas oceânicas. Master's Thesis, Instituto Superior de Engenharia de Lisboa, Lisboa, Portugal, 2017.
26. Hubner, R.G.; Fragassa, C.; da S. Paiva, M.; Oleinik, P.H.; das N. Gomes, M.; Rocha, L.A.O.; dos Santos, E.D.; Machado, B.N.; Isoldi, L.A. Numerical Analysis of an Overtopping Wave Energy Converter Subjected to the Incidence of Irregular and Regular Waves from Realistic Sea States. *J. Mar. Sci. Eng.* **2022**, *10*, 20. [CrossRef]
27. Martins, J.C.; Fragassa, C.; Goulart, M.M.; Santos, E.D.D.; Isoldi, L.A.; Gomes, M.D.N.; Rocha, L.A.O. Constructal Design of an Overtopping Wave Energy Converter Incorporated in a Breakwater. *J. Mar. Sci. Eng.* **2022**, *10*, 471. [CrossRef]
28. Jacobsen, N.G.; Fuhrman, D.R.; Fredsøe, J. A wave generation toolbox for the open-source CFD library: OpenFoam®. *Int. J. Numer. Methods Fluids* **2012**, *70*, 1073–1088. [CrossRef]
29. Higuera, P.; Lara, J.L.; Losada, I.J. Realistic wave generation and active wave absorption for Navier–Stokes models. *Coast. Eng.* **2013**, *71*, 102–118. [CrossRef]
30. Wang, L.; Li, J.; Li, S. Numerical Simulation of Freak Wave Generation in Irregular Wave Train. *J. Appl. Math. Phys.* **2015**, *3*, 1044–1050. [CrossRef]
31. Shen, Z.r.; Wan, D.c. An irregular wave generating approach based on naoe-FOAM-SJTU solver. *China Ocean. Eng.* **2016**, *30*, 177–192. [CrossRef]
32. Dermatis, A.; Ntouras, D.; Papadakis, G. Numerical Simulation of Irregular Breaking Waves Using a Coupled Artificial Compressibility Method. *Fluids* **2022**, *7*, 235. [CrossRef]
33. Carneiro, M.L. Desenvolvimento de dispositivo de geração e absorção ativa de ondas para tanque de ensaios de estruturas oceânicas. Master's Thesis, Escola Politécnica da Universidade de São Paulo, São Paulo, Brazil, 2007.
34. Hirt, C.W.; Nichols, B.D. Volume of fluid (VOF) method for the dynamics of free boundaries. *J. Comput. Phys.* **1981**, *39*, 201–225. [CrossRef]
35. Gomes, M.N.; Lorenzini, G.; Rocha, L.A.; dos Santos, E.D.; Isoldi, L.A. Constructal Design Applied to the Geometric Evaluation of an Oscillating Water Column Wave Energy Converter Considering Different Real Scale Wave Periods. *J. Eng. Thermophys.* **2018**, *27*, 173–190. [CrossRef]
36. Schlichting, H.; Gersten, K. *Boundary-Layer Theory*, 8th ed.; Springer: BurdaBerlin/Heidelberg, Germany, 2000; p. 802. [CrossRef]
37. Lv, X.; Zou, Q.; Reeve, D. Numerical simulation of overflow at vertical weirs using a hybrid level set/VOF method. *Adv. Water Resour.* **2011**, *34*, 1320–1334. [CrossRef]
38. ANSYS Inc. *Ansys Fluent Theory Guide*; ANSYS Inc.: Cannonsburg, PA, USA, 2013.

39. Gomes, M.d.N.; de Deus, M.J.; dos Santos, E.D.; Isoldi, L.A.; Rocha, L.A.O. The choice of geometric constraints value applied in the constructal design for Oscillating Water Column device. In Proceedings of the XXXVIII Iberian Latin American Congress on Computational Methods in Engineering, Florianópolis, Brazil, 5–8 November 2017; pp. 1–17. [CrossRef]
40. Versteeg, H.K.; Malalasekera, W. *An Introduction to Computational Fluid Dynamics*; Pearson: Prentice Hall: Hoboken, NJ, USA, 2007; p. 517.
41. EurOtop. *Manual on Wave Overtopping of Sea Defences and Related Structures. An Overtopping Manual Largely Based on European Research, but For Worldwide Application*; Van der Meer, J.W., Allsop, N.W.H., Bruce, T., De Rouck, J., Kortenhaus, A., Pullen, T., Schüttrumpf, H., Troch, P., Zanuttigh, B., Eds.; Flood and Coastal Erosion Risk Management Research & Development Programme: Bristol, UK, 2018. Available online: http://www.overtopping-manual.com/ (accessed on 15 August 2022).
42. Hervouet, J. *Hydrodynamics of Free Surface Flows: Modelling with the Finite Element Method*; John Wiley & Sons, Ltd.: Hoboken, NJ, USA, 2007. [CrossRef]
43. Oleinik, P.H. Metodologia Numérica para a Simulação Hidrodinâmica de Estados de Mar Utilizando Dados Espectrais e Estudo de Caso de um OWC na Costa de Rio Grande–RS. Master's Thesis, Universidade Federal do Rio Grande, Rio Grande, Brazil, 2020.
44. Tavares, G.P.; Maciel, R.P.; dos Santos, E.D.; Gomes, M.d.N.; Rocha, L.A.O.; Machado, B.N.; Oleinik, P.H.; Isoldi, L.A. A Comparative Numerical Analysis of the Available Power Between Regular and Irregular Waves: Case Study of an Oscillating Water Column Converter in Rio Grande Coast, Brazil. In Proceedings of the 18th Brazilian Congress of Thermal Sciences and Engineering, Online, 16–20 November 2020; p. 11. [CrossRef]
45. Fenton, J.D.; Rienecker, M.M. A Fourier method for solving nonlinear water-wave problems: Application to solitary-wave interactions. *J. Fluid Mech.* **1982**, *118*, 411. [CrossRef]
46. Lisboa, R.C.; Teixeira, P.R.F.; Didier, E. Regular and Irregular Wave Propagation Analysis in a Flume with Numerical Beach Using a Navier-Stokes Based Model. *Defect Diffus. Forum* **2017**, *372*. [CrossRef]
47. Gomes, M.d.N.; Isoldi, L.A.; dos Santos, E.D.; Rocha, L.A.O. Analysis of Grid Refinement for Numerical Generation of Waves in Tanks. In Proceedings of the VII National Congress of Mechanical Engineering, CONEM, Sao Luis, Brazil, 31 July–3 August 2012.
48. Mavriplis, D.J. *Unstructured Mesh Generation and Adaptivity*; Technical report; Program of the von Karman Institute for Fluid Dynamics: Rhode-Saint-Genese, Belgium, 1995.
49. Wave Energy Centre. *Potencial e Estratégia de Desenvolvimento da Energia das Ondas em Portugal*; Technical report; Wave Energy Centre: Lisboa, Portugal, 2004.
50. Halliday, D.; Resnick, R.; Walker, J. *Fundamentals of Physics*, 11th ed.; John Wiley & Sons, Ltd.: Hoboken, NJ, USA, 2018; p. 1456.
51. Jungrungruengtaworn, S.; Hyun, B.S. Influence of slot width on the performance of multi-stage overtopping wave energy converters. *Int. J. Nav. Archit. Ocean. Eng.* **2017**, *9*, 668–676. [CrossRef]
52. Han, Z.; Liu, Z.; Shi, H. Numerical study on overtopping performance of a multi-level breakwater for wave energy conversion. *Ocean. Eng.* **2018**, *150*, 94–101. [CrossRef]
53. Liu, Z.; Han, Z.; Shi, H.; Yang, W. Experimental study on multi-level overtopping wave energy convertor under regular wave conditions. *Int. J. Nav. Archit. Ocean. Eng.* **2018**, *10*, 651–659. [CrossRef]
54. Palma, G.; Formentin, S.M.; Zanuttigh, B.; Contestabile, P.; Vicinanza, D. Numerical Simulations of the Hydraulic Performance of a Breakwater-Integrated Overtopping Wave Energy Converter. *J. Mar. Sci. Eng.* **2019**, *7*, 38. [CrossRef]
55. Barbosa, D.V.E.; Santos, A.L.G.; dos Santos, E.D.; Souza, J.A. Overtopping device numerical study: Openfoam solution verification and evaluation of curved ramps performances. *Int. J. Heat Mass Transf.* **2019**, *131*, 411–423. [CrossRef]
56. Chai, T.; Draxler, R.R. Root mean square error (*RMSE*) or mean absolute error (*MAE*)? – Arguments against avoiding RMSE in the literature. *Geosci. Model Dev.* **2014**, *7*, 1247–1250. [CrossRef]
57. Jin, Y.; Wang, W.; Kamath, A.; Bihs, H. Numerical Investigation on Wave-Overtopping at a Double-Dike Defence Structure in Response to Climate Change-Induced Sea Level Rise. *Fluids* **2022**, *7*, 295. [CrossRef]